

Effect of Annealing Temperature on the Morphology and Sensitivity of the Zinc Oxide Nanorods-Based Methane Sensor

Biplob Mondal · Lachit Dutta · Chirosree Roychaudhury · Dambarudhar Mohanta · Nillohit Mukherjee · Hiranmay Saha

Received: 24 October 2013 / Revised: 19 December 2013 / Published online: 15 July 2014
© The Chinese Society for Metals and Springer-Verlag Berlin Heidelberg 2014

Abstract ZnO nanorods in the form of thin films were synthesized by a facile chemical route and the effect of annealing temperature on the structure and sensitivity of such ZnO-based sensors was studied in detail towards methane sensing. Morphological analyses of such films were carried out by scanning electron microscopy, whereas, the crystalline structure and phase purity of the films were analysed by X-ray diffraction technique. The films were observed to display a gradual change in their morphology from granular to dense nanorods and each of them was used to fabricate methane sensor prototype. They were also tested for temperature-dependent methane-sensing capability with varying methane concentrations. The optimized sensor exhibited highest gas response of $\sim 80\%$ at 250 °C with significantly low response and recovery time.

KEY WORDS: Chemical synthesis; ZnO nanostructures; Thin films; Annealing temperature; Gas sensor; Structural characterization

1 Introduction

Detection of methane in underground coal mines, petroleum industries and gas storage plants is necessary for the

Available online at <http://link.springer.com/journal/40195>

B. Mondal · L. Dutta
Department of Electronics and Communication Engineering,
Tezpur University, Tezpur 784028, Assam, India

C. Roychaudhury
Department of Electronics and Telecommunication Engineering,
Bengal Engineering and Science University, Howrah 711103,
India

D. Mohanta
Nanoscience and Soft Matter Physics Laboratory, Department of
Physics, Tezpur University, Tezpur 784028, Assam, India

N. Mukherjee (✉) · H. Saha
Center of Excellence for Green Energy and Sensors Systems,
Bengal Engineering and Science University, Howrah 711103,
West Bengal, India
e-mail: nilsci@yahoo.co.uk

safety of human beings and environmental control, as it is a highly explosive gas. Metal oxides in the form of nanostructures of specific morphology has become a great deal of interest among researchers because of the possible advantages like high surface-to-volume ratio, appreciable sensitivity, low fabrication cost and potential to provide extremely miniaturized and low-power-consuming sensor. Various metal oxide semiconductors like ZnO, TiO₂, SnO₂, WO₃, In₂O₃, LnFeO₃, etc., have been widely used for sensing gases like hydrocarbons and combustible gases like methane [1, 2], toxic gas like carbon monoxide [3, 5], NO₂ [4], hydrogen [5] and ethane [6]. Their gas-sensing mechanism is governed by the change in electrical conductivity in the presence and/or absence of the test gas. It involves chemisorptions of oxygen on the oxide surface followed by charge transfer during the reaction of the surface absorbed oxygen with target gas molecules. Metal oxide-based sensors can be realized in the form of thick film [7], thin film [8], bulk pellets [9] and nanostructures or nanoparticles. Among the sensors, constructed using nanostructures of metal oxide as the sensing layer were proved to have superior performance [10–13].

Zinc Oxide (ZnO) is a wide band gap n-type semiconductor ($E_g \approx 3.1$ eV at room temperature) with a large free exciton binding energy (60 mV) which has attracted remarkable attention among researchers as sensor material because of its good chemical and thermal stability, sensitivity to different gases, non toxicity, amenability to doping and ease of fabrication [14]. ZnO has been reported to be widely used for sensing hydrocarbons and combustible gases like H_2 [15], CH_4 [16], LPG [17], CO [18].

Sensing characteristics of chemical sensors depend on the morphology and surface-to-volume ratio of the sensing layer. Nanostructured ZnO in the form of nanobelts, nanorods, nanowires, etc., shows superior response to target gas owing to their larger surface-to-volume ratio, thereby allowing greater exchange of charge carriers during oxidation/reduction mechanism [10–13]. Lots of studies were reported focussing on the enhancement of gas response by decreasing the size of the nanoparticles [19], the diameter of nanowires [20], and thickness of the nanosheets [21]. Nanostructured ZnOs synthesised by various physio-chemical techniques in various forms such as nanowire, nanoflowers, nanopillar, nanotetrapods, nanorods. were also investigated by various authors. A summary of ZnO nanostructures and their response to different target gases is presented in Table 1. ZnO nano-material-based methane sensors have also been reported by various authors [1, 30–32].

In this contribution, we propose a simple chemical route to prepare rod-like ZnO nanostructures. Effect of annealing temperature on the crystallinity, size and density of nanostructures has been investigated. The ZnO nanorods were used to construct gas sensor and response of the sensor to varied concentration of methane at different operating temperatures was also studied.

2 Experimental

2.1 Synthesis of ZnO Nanostructures

The flowchart for the synthesis of ZnO nanorods by the technique reported here is shown in Fig. 1. Polyvinyl alcohol (PVA) was chosen as the supporting matrix for embedding ZnO nanostructures. PVA solution (5 wt%) was prepared by vigorous stirring of the PVA and distilled water at 500 r/min for 3 h, while maintaining a temperature of 60 °C until a transparent viscous solution was obtained. After that, 0.60 g of zinc acetate dihydrate [$Zn(CH_3COO)_2 \cdot 2H_2O$] was added to the aqueous solution of PVA with continuous stirring. 1.0 mol/L NaOH solution was prepared separately by dissolving 0.40 g of NaOH in 10 mL distilled water, which was added drop wise to the solution under continuous stirring at 80 °C maintaining the final pH value of the solution at 8.0.

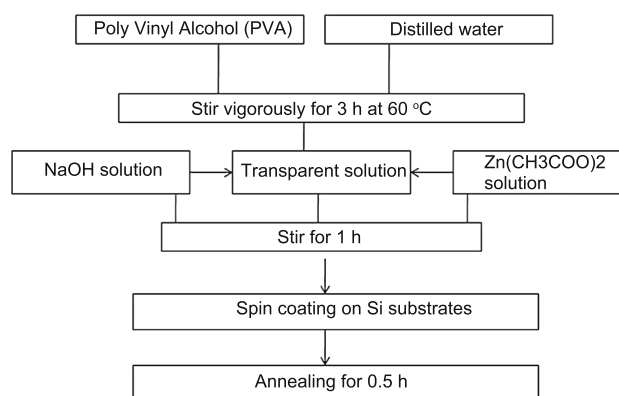
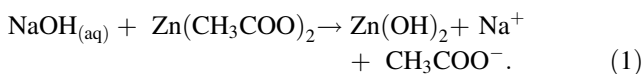


Fig. 1 Flowchart illustrating the steps in the chemical synthesis of ZnO nanorods

Table 1 Summary of gas response of ZnO nanostructured sensor

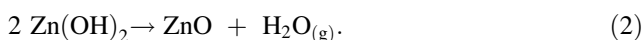
Morphology	Method of preparation	Target gas	Sensor temperature (°C)	Gas concentration (ppm)	Response	Ref.
Nanopillar	Solution growth	Ethanol and H_2	350	100	18.3 (ethanol) 10.4 (H_2)	[22]
Nanotetrapod	Thermal evaporation	Ethanol	300	100	~ 29.4	[13]
Nanorod	Hydrothermal	H_2S	27	0.05	~ 1.7	[23]
Nanowire	Thermal evaporation	Ethanol	300	100	~ 33	[24]
Nanoplate	Solution growth/ thermal annealing	Ethanol and chlorobenzene	200 (chlorobenzene) 300 (ethanol)		~ 6.9 (chlorobenzene) ~ 8.9 (ethanol)	[25, 26]
Nanoflower	Hydrothermal	–				[27, 28]
Nanofibre	Electrospinning	Ethanol	200	10	~ 0.89	[20]
Nanotube	Spray pyrolysis then oxidation	H_2	200	1000	~ 740	[29]

The following reaction is proposed to take place in the bath:



The resulting precursor was spin casted onto a cleaned (100) oriented Si/SiO₂ substrate at 1000 r/min for 60 s, followed by annealing in air at 400, 550 and 700 °C, each for 30 min in a quartz tube furnace. The temperature of the furnace was ramped at 1.5 °C/s and was cooled down to room temperature at the same cooling rate to avoid generation of cracks on the films.

When the as-deposited material is annealed at higher temperature, the following reaction takes place to produce crystalline ZnO from the amorphous Zn(OH)₂:



2.2 Characterization Techniques

The structure and the phase of the deposited materials (both as deposited and annealed) were determined by X-ray diffraction technique (XRD, RIGAKU-MINIFLUX, using CuK_α radiation ($\lambda = 0.1540598$ nm) with 30 kV, 15 mA), at a scan rate of 1°/min and within 2θ in the range of 20°–60°. The morphology of the materials were determined by scanning electron microscopy (SEM; JEOL JSM 6390LV, operating at 15 kV). An electrometer (Keithley® 2400) was used to monitor the variation of sensor resistance.

2.3 Sensor Architecture and Testing Methods

The schematic of the sensor device is shown in Fig. 2. The sensor is designed to operate in a resistive mode. It consists of ZnO nanorods grown over a Si/SiO₂ substrate (1.5 cm × 1.0 cm). Pd–Ag contact electrodes were made on the top of the ZnO layer by e-beam evaporation technique. The contact dimension was 2 mm × 2 mm and the average distance between two lateral contacts was 5 mm. The sensors fabricated from the ZnO nanorods annealed at 400, 550 and 700 °C were labelled as sensor I, sensor II and sensor III, respectively.

The gas-sensing properties of the proposed sensors were studied by two probe *I–V* measurements technique using custom-made sensor characterization setup as shown in Fig. 2 and by varying the methane gas concentration and measurement conditions, as well. The sensor was placed inside an enclosed test chamber with provision for heating arrangement that would maintain a uniform temperature environment (with an accuracy of ±3 °C) inside the chamber. Ultra-high pure methane diluted with air is fed to the sensor in appropriate concentration through Alicat® mass flow controllers (MFC). An electrometer (Keithley®

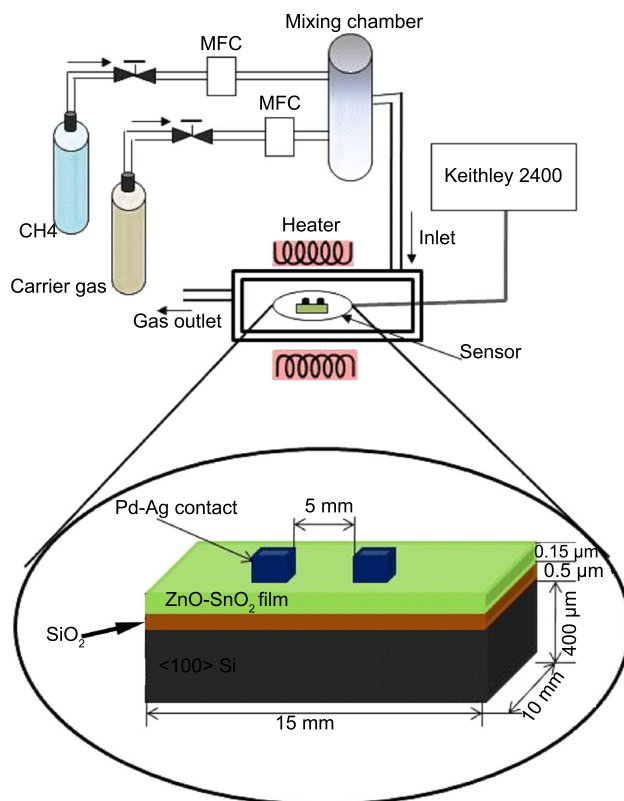


Fig. 2 Schematic of the sensor structure

2400) was used to monitor the variation of sensor resistance. The sensor performance was examined within 0.1%–1.0% of methane gas in air at room temperature and also at higher temperatures (300 °C).

3 Results and Discussion

3.1 Structural Characterization by X-ray Diffraction (XRD) Study

XRD analysis was carried out to identify the crystalline structure and phase of the as-prepared and annealed samples. Figure 3 illustrates the XRD patterns of the as-deposited and annealed (at 400, 550 and 700 °C) samples. The XRD pattern for the as-deposited material (Fig. 3a) was amorphous in nature and without any significant peak corresponding ZnO. This indicates the deposition of precursor Zn(OH)₂ at the initial stage, which is amorphous in nature. On annealing the films at higher temperatures, crystallinity comes up gradually (Fig. 3b–d) with the most preferred orientation to (002) plane for ZnO. Maximum crystallinity was observed for the sample annealed at 700 °C, where major diffractions from (100), (002), (101) and (102) planes were observed, which matched well with

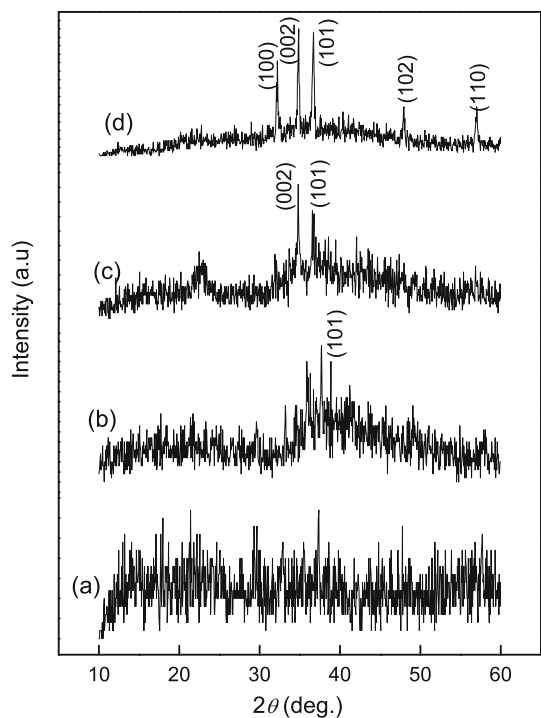


Fig. 3 X-ray diffraction patterns of as-deposited sample **a**, samples annealed at 400 °C **b**, 550 °C **c**, 700 °C **d**

the hexagonal (wurtzite) structure of ZnO (JCPDS card No. 36-1451). The decrease in full width at half maxima (FWHM) of the XRD peaks with increasing annealing temperature indicates the increasing of the crystallinity of the deposited material with temperature.

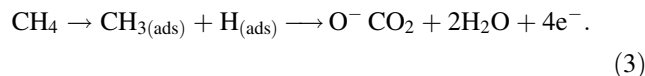
3.2 Morphological Analysis by SEM

The surface morphology, size and distribution of the ZnO particles were studied by SEM. Figure 4a shows the SEM image of the as-prepared layer obtained by spin coating, which reveals the formation of a seed layer with an average particle size of 40–60 nm. Some regions of overgrowth were also observed from the SEM image of the spin-coated layer. Figure 4b–d represent the morphologies of the samples annealed at 400, 550 and 700 °C, respectively. The decomposition temperature of PVA is 300 °C, below which no formation of ZnO nanorods will be observed, and this temperature has been established as the critical temperature for the formation of ZnO nanorods. At an annealing temperature of 400 °C, the decomposition and removal of PVA occurs, and the formation of ZnO nanorods starts. At this temperature, the length and breadth of such a nanorod were found to be 700–900 and 60–90 nm. On further increasing the annealing temperature to 700 °C, the length of the nanorods was also found to increase in the range of

1.2–1.5 μm. The diameter of the nanostructure also increased from 60–90 nm for the sensors I and II to approximately 200 nm for sensor III. It was also noted that only a few nanorods were visible on the sample annealed at 400 °C. An enormous increase in density of the nanorods was observed with the increase of annealing temperature to 700 °C which is due to the fact that at higher temperature, complete removal of the polymer matrix occurs which facilitates the ZnO crystal growth [33].

3.3 Methane Sensor Prototype

The gas-sensing properties of annealed ZnO nanorods were studied through two probe *I–V* measurement technique (resistive mode) with due emphasis on operating temperature and gas concentration dependencies. The temperature was varied from 75 to 300 °C, whereas gas concentration was varied within 0–1.0% with diluted air as the carrier gas. The response magnitude, response and recovery times were calculated from the experimental data. The typical physio-chemical reaction mechanism may be described as [1]



The sensitivity of the sensors to the varying concentration of methane gas is determined from the recorded *I–V* data. The response magnitude of a semiconductor gas sensor is defined as

$$S = [R_{\text{air}} - R_{\text{gas}}] / R_{\text{air}} \quad (4)$$

Figure 5a–c show the *I–V* characteristics of the sensors at different temperatures (within 75–300 °C) for a constant concentration (1.0%) of methane gas. As can be seen, the current traces basically exhibit sub-linear dependencies in response to the applied voltage. The responses were found to be higher at higher voltages, temperatures and gas concentrations. In other words, corresponding to a definite temperature, current transport is purely governed by gas adsorption, leading to the release of conduction electrons which ultimately participate in the transport process. The non-linear behaviour of the *I–V* curve reveals the formation of Schottky junction between ZnO nanorods and palladium-silver top contact.

The sensor shows an increasing trend of the conductance ($\Delta I / \Delta V$) with methane concentration, which is plotted in Figs. 6a–c. This is because more free electrons are released as a result of enhanced reaction between the increased methane gas concentration and adsorbed oxygen as per

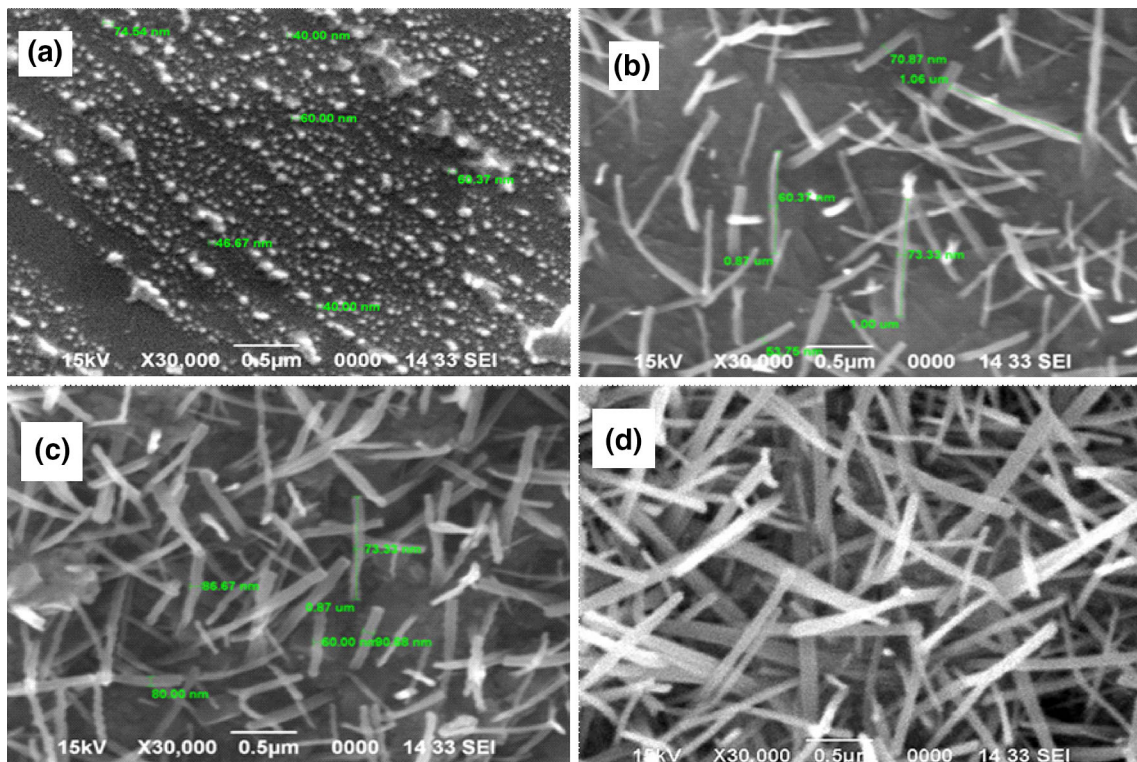


Fig. 4 SEM images of ZnO nanorod as deposited **a**, annealed at 400 °C **b**, 550 °C **c**, 700 °C **d**

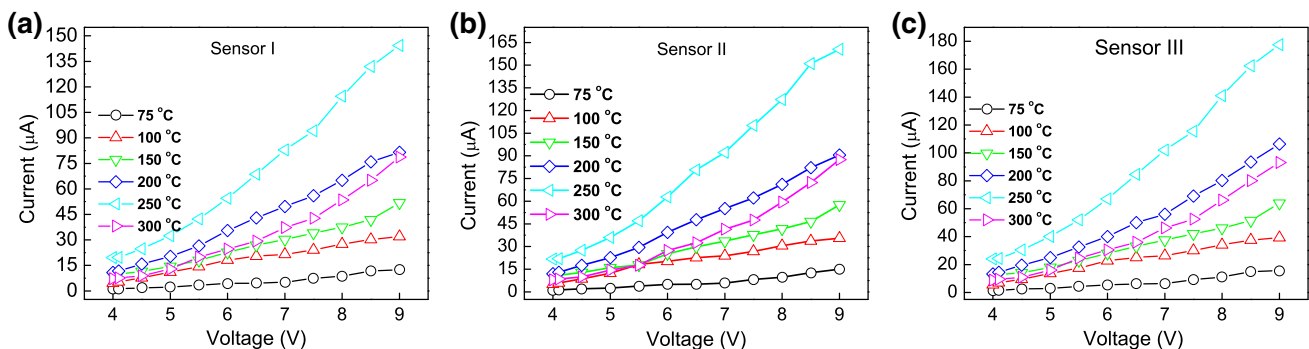


Fig. 5 *I*–*V* characteristics of sensor prototypes I **a**, II **b**, III **c** at different operating temperatures

Eq. (3). The sensor presents highest conductance at 250 °C and the order is:

$$\begin{aligned}
 (\Delta I/\Delta V)|_{250^\circ\text{C}} &> (\Delta I/\Delta V)|_{200^\circ\text{C}} > (\Delta I/\Delta V)|_{150^\circ\text{C}} \\
 &> (\Delta I/\Delta V)|_{100^\circ\text{C}} > (\Delta I/\Delta V)|_{75^\circ\text{C}}.
 \end{aligned}
 \tag{5}$$

The conductance saturates beyond a critical value due to the lack of adequate adsorbed oxygen molecules to react with CH₄. It is known that oxygen molecules can be adsorbed onto the surface of ZnO layer thereby forming oxygen ions (O⁻, O₂⁻, O²⁻) and finally, extracting out electrons [1]. When methane comes in contact with the sensor, it tends to react with the adsorbed oxygen ions. As a result, the

adsorbed oxygen is released from the ZnO layer and consequently re-injecting electrons following Eq. (3), leading to an increase in the conductivity of the sensor. Upon optimal surface adsorption of CH₄ molecules on the ZnO surface, the release of free electron gets suppressed. This is the reason why the rise of conductance ceases beyond a certain limit. It was also noted that the ZnO nanorods-based sensor annealed at 700 °C had highest conductance compared to those annealed at 400 and 550 °C. This is because; the number of the nanorods per unit area is highest for the samples annealed at 700 °C and lowest at 400 °C, as can be seen from the SEM images (Fig. 4).

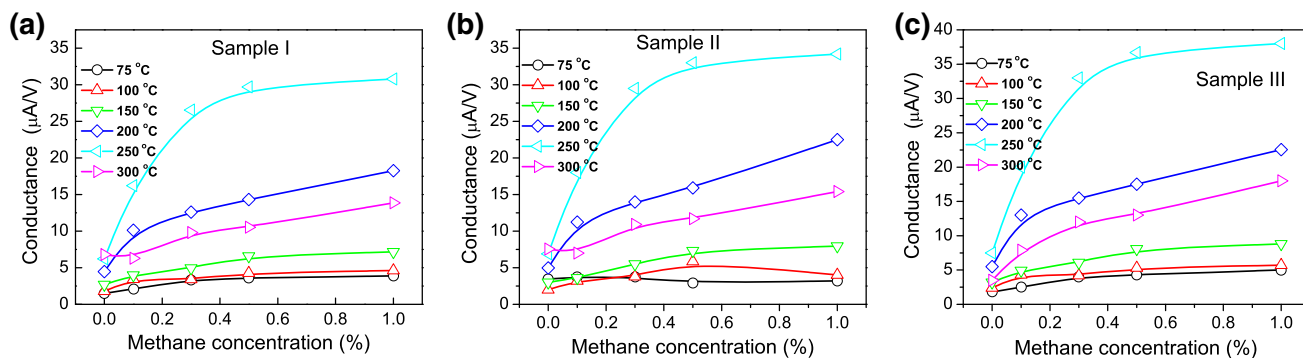


Fig. 6 Variation of conductance ($\Delta I/\Delta V$) with methane concentration for sensor I **a**, sensor II **b**, sensor III **c**

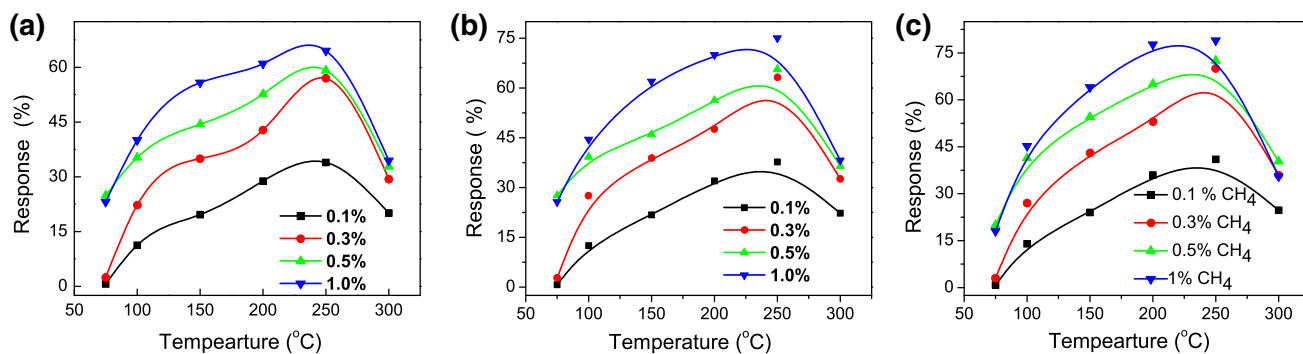


Fig. 7 Response vs. operating temperature at varied methane concentration for sensor I **a**, sensor II **b**, sensor III **c**

The on-off switching and the sensitivity study of the sensors were performed for the highest concentration (1.0%) of methane. Sensitivity of a gas sensor is also dependent on the operating temperature as mentioned in the previous discussion (Eq. (5)). The dependence of sensor response on the operating temperature (for varying concentration of methane and at a bias) is plotted in Fig. 7, from which, it is evident that the sensors had a maximum response of 64% (sensor I), 75% (sensor II) and 80% (sensor III) at 250 °C for 1.0% methane. The sensor response increased rapidly with the rise of temperature until an optimum operating temperature is reached, after which the response decreases. This behaviour can be explained by analogy with the gas adsorption mechanism on metal oxide surface [34]. In ambient environment, an *n*-type metal oxide like ZnO preferentially adsorbs O_2^- below 100 °C, O^- between 100 and 300 °C, and O^{2-} species above 300 °C [35]. The adsorbed oxygen in the form of O^- makes the sensor material most sensitive because this O^- is the most reactive one among the three. At temperature below 100 °C, surface preferentially adsorbs O_2^- ions and the sensitivity of the sensor is small. As the temperature increases, the surface adsorbs O^- ions, leading to an increase in the sensitivity.

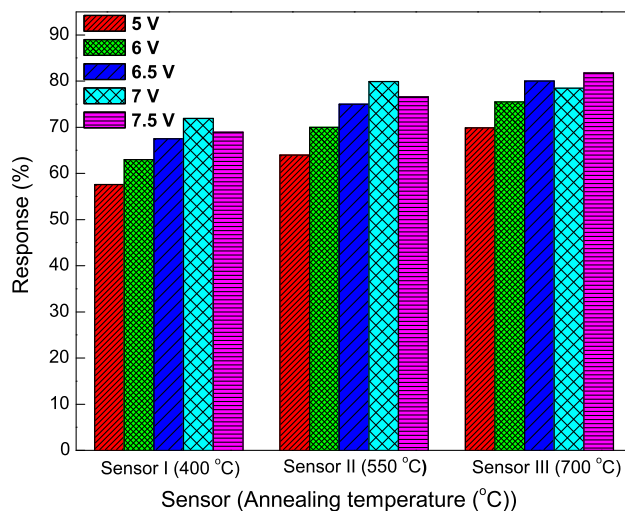


Fig. 8 Response of the annealed samples at different bias voltages (operating temperature is 250 °C) at 1.0% methane

The sensor response for varied bias voltage at 1.0% methane concentration is also plotted in Fig. 8. Response is seen to be higher at higher voltage. This is due to the fact that the sensor base resistance is a function of the applied

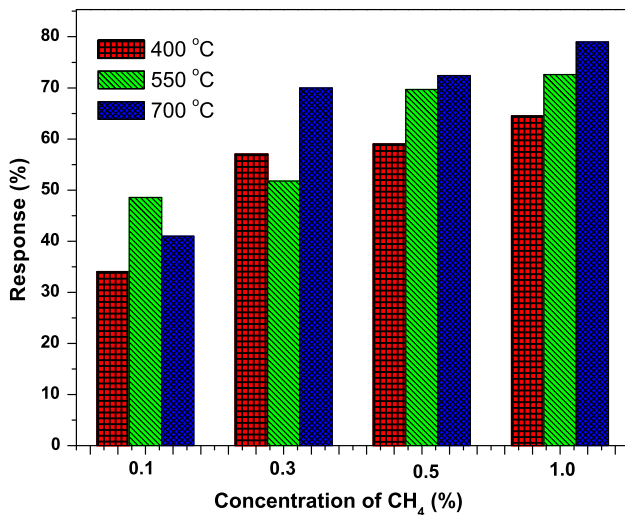


Fig. 9 Response versus methane gas concentration for the annealed samples (operating temperature is 250 °C)

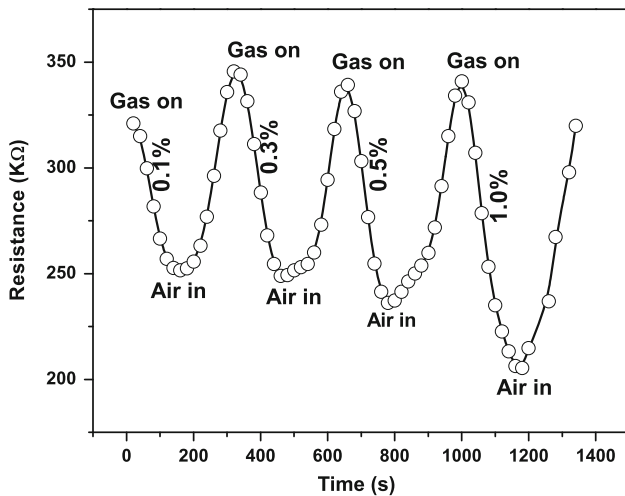


Fig. 10 Dynamic response of ZnO nanorod-based sensor (sensor II) at 250 °C in 1.0% methane

bias as can be examined from the non-linear *I–V* characteristics (Fig. 6) which might be due to the high diffusivity of silver through zinc matrix. The sensor base resistance

was found to drop as the bias voltage is increased, which causes a much higher current to flow through the sensor. Hence the response increases at higher applied bias.

The uptake gas concentration vs. sensor response at the operating temperature of 250 °C is shown in Fig. 9. In general, the response has an increasing trend with increasing gas concentration. In all these cases, however, there is a saturation trend beyond a critical concentration.

The dynamic response and recovery curve of the ZnO nanorods-based sensors to 1.0% methane gas at 250 °C for sensor II are shown in Fig. 10. From the recorded data, it is seen that as the sensor is exposed to the test gas, the sensor current increases and then tends to return to the baseline when the gas is ‘out’, exhibiting a clearly repeatable sensing activity. The response time is defined as the time required for reaching 90% of the equilibrium value of the resistance after gas exposure, and the recovery time is defined as the time required for the resistance to return to 10% above original resistance in air after test gas is out [36]. While exhibiting a clear repeatability to gas sensing and conductance change, minimum response time and recovery time, as calculated, were found to fall in between 91–120 and 121–170 s, respectively, as shown in Table 2.

At a certain temperature, ZnO traps molecular oxygen from air in the form of O⁻ or O²⁻ on its surface. The electrons of O⁻ or O²⁻ come from the bulk of the n-ZnO and such trapping of the electrons by O⁻ or O²⁻ on the surface of the semiconductor increases the resistance. When the target gas comes on the surface of the ZnO layer, it reacts with the O⁻ or O²⁻ (in this case O⁻) and the trapped oxygen releases the electrons on the surface of ZnO, and thus the resistance decreases. When the gas is purged by air (which contains oxygen) then ZnO again starts to absorb the molecular oxygen. But at the beginning of the second cycle, the electron density of the ZnO surface is already higher by the electrons released at first cycle. So, some extra electrons come from the bulk of the semiconductor to the surface to absorb oxygen species, which in turn lowers the electron concentration in the bulk of the semiconductor and increases the base resistance at the beginning of the second gas in–out cycle.

Table 2 Response and recovery time of the ZnO nanorod-based sensor prototype annealing at different temperatures when subject to methane with different concentrations

Annealing temperature (°C)	Response time (s)				Recovery time (s)			
	0.1%	0.3%	0.5%	1%	0.1%	0.3%	0.5%	1%
400	107	108	113	120	139	158	163	170
550	100	100	105	110	130	150	155	160
700	93	91	97	92	121	140	142	149

4 Conclusions

Zinc oxide-based methane gas sensor fabricated by thermal annealing method has been demonstrated here. The effect of annealing temperature on the crystalline structure, phase and microstructure of the deposited material was investigated by XRD and SEM, respectively, which confirms the growth of hexagonal wurtzite ZnO nanorods. The response of the sensor constructed using the annealed samples was studied for varied concentration of methane gas (0.1%–1.0%) at different operating temperatures. The study revealed that the optimum operating temperature of the sensor was 250 °C at which the highest achieved response was ~80%. The sensor prototype exhibited a clearly repeatable sensing activity with minimum response and recovery time of 90 and 120 s, respectively.

References

- [1] P. Bhattacharyya, P.K. Basu, B. Mondal, H. Saha, *Microelec. Reliability* **48**, 1772 (2008)
- [2] P. Bhattacharyya, P.K. Basu, H. Saha, S. Basu, *Sens. Actuators, B* **124**, 62 (2007)
- [3] E. Comini, G. Faglia, G. Sberveglieri, Z. Pan, Z. Wang, *Appl. Phys. Lett.* **81**, 1869 (2002)
- [4] J. Polleux, A. Gurlo, N. Barsan, U. Weimar, M. Antonietti, M. Niederberger, *Angew. Chem.* **45**, 261 (2006)
- [5] V.V. Sysoev, B.K. Button, K. Wepsiec, S. Dmitriev, A. Kolmakov, *Nano Lett.* **6**, 1584 (2006)
- [6] H.T. Giang, H.T. Duy, P.Q. Ngan, G.H. Thai, D.T.A. Thu, D.T. Thu, N.N. Toan, *Sens. Actuators, B* **158**, 246 (2011)
- [7] G. Rao, D. Rao, *Sens. Actuators, B* **23**, 181 (1999)
- [8] A.P. Chatterjee, P. Mitra, A.K. Mukhopadhyay, *J. Mater. Sci.* **34**, 4225 (1999)
- [9] G.J. Li, X.H. Zhang, S. Kawi, *Sens. Actuators, B* **60**, 64 (1999)
- [10] N. Mukherjee, Sk.F. Ahmed, K.K. Chattopadhyay, A. Mondal, *Electrochim. Acta* **54**, 4015 (2009)
- [11] J. Xu, Y. Chen, Y. Li, J. Shen, *J. Mater. Sci.* **40**, 2919 (2005)
- [12] P. Bhattacharyya, P.K. Basu, N. Mukherjee, A. Mondal, H. Saha, S. Basu, *J. Mater. Sci. Mater. Electron.* **18**, 823 (2007)
- [13] C. Xiangfeng, J. Dongli, A.B. Djuricic, Y.H. Leung, *Chem. Phys. Lett.* **401**, 426 (2005)
- [14] S.J. Pearton, D.P. Norton, K. Ip, Y.W. Heo, T. Steiner, *J. Vac. Sci. Technol. B* **22**, 932 (2004)
- [15] S.N. Das, J.P. Kar, J.H. Choi, T.I. Lee, K.J. Moon, J.M. Myoung, *J. Phys. Chem. C* **114**, 1689 (2010)
- [16] D. Gruber, F. Kraus, J. Muller, *Sens. Actuators B* **92**, 81 (2003)
- [17] C.S. Prajapati, S.N. Pandey, P.P. Sahay, *Phys. B* **406**, 2684 (2011)
- [18] R.K. Joshi, Q. Hu, F. Alvi, N. Joshi, A. Kumar, *J. Phys. Chem. C* **113**, 16199 (2009)
- [19] T. Kida, T. Doi, K. Shimanoe, *Chem. Mater.* **22**, 2662 (2010)
- [20] Y. Zeng, T. Zhang, L. Qiao, *Mater. Lett.* **63**, 843 (2009)
- [21] C.S. Moon, H.R. Kim, G. Auchterlonie, J. Drennan, J.H. Lee, *Sens. Actuators B* **131**, 556 (2008)
- [22] L.J. Bie, X.N. Yan, J. Yin, Y.Q. Duan, Z.H. Yuan, *Sens. Actuators B* **126**, 604 (2007)
- [23] Q. Wang, X. Chu, M. Wu, *Sens. Actuators B* **113**, 320 (2006)
- [24] Q. Wan, Q.H. Li, Y.J. Chen, T.H. Wang, X.L. He, J.P. Li, C.L. Lin, *Appl. Phys. Lett.* **84**, 3654 (2004)
- [25] A. Zuo, P. Hu, L. Bai, F. Yuan, *Cryst. Res. Technol.* **44**, 613 (2009)
- [26] Z. Zing, J. Zhan, *Adv. Mater.* **20**, 4547 (2008)
- [27] R. Yi, N. Zhang, H. Zhou, R. Shi, G. Qui, *Mater. Sci. Eng. B* **153**, 25 (2008)
- [28] L. Jiang, G. Li, Q. Ji, H. Peng, *Mater. Lett.* **61**, 1964 (2007)
- [29] C.S. Rout, S.H. Krishna, S.R.C. Vivekchand, A. Govindaraj, C.N.R. Rao, *Chem. Phys. Lett.* **418**, 586 (2006)
- [30] P.K. Basu, S.K. Jana, H. Saha, S. Basu, *Sens. Actuators B* **135**, 81 (2008)
- [31] A. Sengupta, S. Maji, H. Saha, *Adv. Sci. Lett.* **3**, 385 (2010)
- [32] P. Bhattacharyya, P.K. Basu, L.C. Lang, H. Saha, S. Basu, *Sens. Actuators B* **129**, 551 (2008)
- [33] Y. He, W. Sang, J. Wang, R. Wu, J. Min, *J. Nanopart. Res.* **7**, 307 (2005)
- [34] Y. Wang, X. Wu, Y. Li, Z. Zhou, *Solid-State Electron.* **48**, 627 (2004)
- [35] M. Takata, D. Tsubone, H. Yanagida, *J. Am. Ceram. Soc.* **59**, 4 (1976)
- [36] W.Y. Wu, J.M. Ting, P.J. Huang, *Nanoscale Res. Lett.* **4**, 513 (2009)